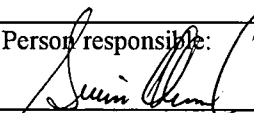


NGU Report 95.152

Fluorine-rich biotites and alkali-metasomatism as
guides to massive sulphide deposits: an example
from the Bleikvassli Zn-Pb-Ag-(Cu) deposit,
Norway

Report no.: 95.152		ISSN 0800-3416	Grading: open
Title: Flourine-rich biotites and alkali-metasomatism as guides to massive sulphide deposits: an example from the Bleikvassli Zn-Pb-Ag-(Cu) deposit, Norway			
Authors: Rune B. Larsen, Nicholas Walker, Anne Birkeland and Terje Bjerkgård		Client: NGU, The Nordland Programme, Bleikvassli Gruber	
County: Nordland		Commune: Hemnes	
Map-sheet name (M=1:250.000) Mosjøen		Map-sheet no. og -name (M=1:50.000) 1926-I, Røsvatnet	
Deposit name and grid-reference: Bleikvassli deposit (65°55'24" N, 13°52'47" E)		Number of pages: 37	Price (NOK): 55
		Map enclosures: 0	
Fieldwork carried out: 1993, 1994, 1995	Date of report: 15 December, 1995	Project no.: 00.2543.29	Person responsible: 
Summary: The Bleikvassli massive sulphide deposit is closely associated with a microcline gneiss interpreted as the metamorphosed equivalent of an alkaline magmatic rock of syenitic composition which yield a concordant U/Pb zircon age of 481 ±2 Ma. A 30 metres wide zone along the margin of the microcline gneiss suffered intensive alkali-depletion and addition of iron and magnesium, when it was metamorphosed together with the massive sulphides. Iron and magnesium partitioned in to biotite and phengitic mica and biotite show a conspicuous enrichment of fluorine and depletion of iron compared to the unaltered interior of the microcline gneiss. Partitioning of fluorine in favour of biotite is an indirect effect of the proximity to the massive sulphides. This is because an environment with a high f_{S_2} will favour the crystallisation of phlogopitic biotites which will enhance the substitutional exchange of F ⁻ for OH ⁻ . Because of this effect, fluorine can be used as a guide revealing the existence of unexposed massive sulphide deposits.			
Keywords: Massive sulphides	Exploration	Flourine-rich biotites	
Alkali-metasomatism	Zn	Pb	
Cu	Ag	Microcline gneiss	

1 CONTENTS

1 CONTENTS	3
2 FIGURES	4
3 TABLES	4
4 APPENDIX.....	5
5 INTRODUCTION.....	6
6 GEOLOGICAL SETTING.....	6
7 MICROCLINE GNEISS.....	7
8 PETROGRAPHY.....	8
9 WHOLE ROCK CHEMISTRY	8
10 EMP-ANALYSIS	9
11 GEOCHRONOLOGY	10
12 DISCUSSION	10
13 APPLICATION TO EXPLORATION	12
14 CONCLUSION.....	13
15 ACKNOWLEDGEMENT.....	13
16 REFERENCES.....	14

2 FIGURES

Figure 1: Geological setting of the studied area. The Anders Larsa Group includes the marbles and all the units NW of this. All the samples employed in this study were obtained from profile 1. Geological map is compiled and modified after data from Ramberg (unpublished data), Olsen (1984), Larsen (1984) and Skauli (1990).

Figure 2: Major and minor element geochemistry based on whole rock XRF analysis of altered and unaltered samples of the microcline gneiss except from Fig. 2a and 2b where only unaltered samples has been included.

Figure 3: Variations in major and minor elements along profile 1 in the microcline gneiss. Position of the Bleikvassli massive sulphide deposit corresponds to 0 metres.

Figure 4: Pearce Element Ratio analysis (PER) of altered and unaltered samples from the microcline gneiss. Samples that are deviating from the straight lines suffered post magmatic alteration.

Figure 5: Electron microprobe analysis of biotite and muscovite from close to the massive sulphide/microcline gneiss intersection (0 m) and in to the interior of the microcline gneiss.

Figure 6: Electron microprobe analysis showing the concentration of fluorine as a function of the iron content of the biotites.

Figure 7: Concordia diagram showing the results of U/Pb dating of zircon separates from the microcline gneiss. Only upper concordia intercept is shown on diagram.

Figure 8; f_{S_2} - f_{O_2} diagram showing the stability of biotite as a function of the oxygen fugacity and the sulphur fugacity at 550 °C and 6 kbar pressure. Numbers in bold and in brackets denotes the mole fraction of Fe and the concentration by weight of F, respectively, in the biotite. Numbers in brackets show the concentration of fluorine in biotites from the microcline gneiss. Shaded area indicate the conditions under which biotites in the microcline gneiss could have crystallised. Partially adapted from Nesbitt (1985).

3 TABLES

Table 1: XRF analysis, representative samples from unaltered and altered microcline gneiss and examples from the literature.

Table 2: Representative EMPA analysis of biotite and muscovite from the microcline gneiss.

Table 3: Analytical data relevant to the U/Pb determinations.

4 APPENDIX

Appendix 1: XRF analysis of whole rock samples from the microcline gneiss.

Appendix 2: EMPA analysis of biotite and muscovite from profile 1.

5 INTRODUCTION

The Bleikvassli massive sulphide deposit is an actively mined sediment hosted massive Zn-Pb-Ag-(Cu) ore situated in the Caledonide part of north Norway (65°55'24'' N and 13°52'47'' E). Being an integrated part of the Uppermost Allochthon, this deposit has been exposed to multiple episodes of high grade pre- and syn-Caledonian metamorphism and deformation. Metamorphism and deformation imposes serious problems for the discovery of syn-genetic alteration features associated with the massive sulphides; features which otherwise can be used as an aid in the exploration for hidden ore deposits. An alternative approach is to explore for metamorphogenic alteration phenomena, because metamorphism of massive sulphide deposits can superimpose a secondary sulphidation-oxidation halo in the adjacent host rock. This approach is currently investigated by Spry and co-workers (1995) to constrain the extent of metamorphogenic oxidation and sulphidation of the hanging wall lithologies of the Bleikvassli deposit. In the present study we have investigated the alteration phenomena that is caused by syn-metamorphic fluid-rock interaction between metasomatising fluids, the massive sulphides and a microcline gneiss. Furthermore, we wish to evaluate the possibilities of using these alteration features as an aid in future exploration after massive sulphide deposits. The microcline gneiss provides us with an excellent opportunity to study the mass balance budget during syn-metamorphic ore-rock interaction. This is because only parts of the microcline gneiss exchanged matter with the ore body which consequently leaves us with a reference level corresponding to the un-metasomatised interior of the gneiss

6 GEOLOGICAL SETTING

The massive sulphide occurrences in the Bleikvassli area are located in the Eastern part of the Rødingsfjell nappe complex which is a part of the Uppermost Allochthon of the Scandinavian Caledonides (Stephens et al., 1985) (Figure 1). This part of the allochthon is composed of basinal clastic meta-sediments belonging to the Kongsfjellet and Anders Larsa Groups. By far the majority of the Kongsfjellet Group is composed of kilometres thick and laterally persistent units of garnet-mica schist intercalated with calcareous schist, amphibolites and minor calcite marbles (Ramberg, 1967; Bjerkgård et al. *in prep*). Toward the stratigraphic top of the Kongsfjellet Group, at the transition to the overlying Anders Larsa Group, the lithologies become more heterogeneous with intercalations of amphibolites, quartzo-feldspatic schists, graphitic schists and marbles (figure 1). At this level, where the massive sulphide occurrences are situated, more exotic rocks appear in the stratigraphy including tourmalinites, feldspatic gneisses, calc-silicate rocks and schists with up to 60 vol. % white kyanite. Continuing in to the Anders Larsa Group, the stratigraphy becomes dominated by massive, up to several hundred metres thick calcite and dolomite marbles intercalated with garnet-mica schists, amphibolites and calc-silicate rocks. Recently, regional geological mapping has shown that the Kongsfjellet and Anders Larsa Groups can be traced along strike for 60 kilometres and can be correlated with the Plurdalen Group North of the studied area (Bjerkgård et al. *in prep*). As a consequence, the entire stratigraphy define a considerable meta-sedimentary basin reaching a thickness of several kilometres over an area of >2000 km². This basin was situated in a marginal continental setting (Marker, 1983). ⁸⁷Sr/⁸⁶Sr isotope analyses of marbles from the Anders Larsa Group uniformly indicates an age between 590 and 600 Ma when compared to the strontium isotope curve for marine carbonates (Bjerkgård et al., *in prep*). These ages are comparable with marbles from the Helgeland nappe complex, that also belongs to the Uppermost Allochthon (Trønnes and Sundvold, 1995). Rb/Sr whole rock geochronology (Marker, 1983) on a meta-granite intrusions and a concordant U/Pb zircon age on a gabbroic intrusion (Senior and Andriessen, 1990), constrain the upper age of the Rødingsfjell

Complex, including Plurdalen, Kongsfjell and Anders Larsa Groups to 572 ± 32 and 576 ± 7 Ma, respectively.

Pre- and syn-Caledonian cross folding with E-W trending fold axis, began with two events of isoclinal folding, and continued in to the F_3 phase characterised by mega-scale closed recumbent folds. F_1 to F_3 were overprinted by open F_4 folds which, finally, was followed by an episode of gentle F_5 folds following the main Caledonian N-S direction (Marker, 1983; Larsen, 1984; Olsen, 1984; Rasmussen, 1984; Seir 1985; Bjerkgård et al., *in prep*). Metamorphism reached upper amphibolite facies and, in the Bleikvassli area, peak conditions corresponds to 540° - 570° C and 7.5-7.9 Kb (Cook, 1993).

The Bleikvassli massive sulphide deposit is situated close to the hinge zone of a mega-scale recumbent north form (F_3) where 6 mill. tons of recoverable ore has been proven so far. Smaller dragfolds along the upper limb of this structure locally multiply the thickness of the massive sulphides to >10 metres in the southern end of the ore body, whereas the thickness of the northern part of the ore-body reach 2-3 metres. According to the classical studies of Vokes (1963), the deposit can be divided in to a pyrrhotite rich south- and a more pyrite rich north ore body, also corresponding to the proximal and distal part of the deposit, respectively. Sphalerite and galena are the dominant economic minerals but chalcopyrite, though sub-economic, is particularly common in the south ore-body. Besides Pb and Zn, Ag and occasionally Au are recoverable metals yielding average grades of 3 and 8 %, 45 ppm and 231 ppb, respectively. Recent studies have documented that the Bleikvassli ore-deposit should be regarded as a sedimentary exhalative massive sulphide deposit (SEDEX) given its meta-sedimentary setting, distribution of ore-forming elements and relationship with the host rock (Skauli, 1990). A more detailed account addressing mineralogy, geochemistry and effects of metamorphism, can be found in Vokes (1963, 1966, 1968, 1969, 1976), Ramberg (1967) and Skauli (1990, 1992a, 1992 b).

7 MICROCLINE GNEISS

The following description will focus on the field relations, structures and textures of the microcline gneiss as it appears along a profile extending from the contact toward the Bleikvassli massive sulphides and 70 metres in to the gneiss (profile 1 on Fig. 1). Particular attention is given to the micas because their composition and textural relationship will be used extensively throughout this study. A comprehensive description of the other varieties of feldspatic gneisses in the Bleikvassli area, can be found in Skauli (1993).

The microcline gneiss is a characteristic felsic body situated between a garnet-mica schist and the kyanite schist described in the previous section (Fig. 1). Toward the SW, an arm of the Bleikvassli deposit wedge in to the contact between the microcline gneiss and the kyanite schist. The ore-body is not in direct contact with either of the two units but is separated from the gneiss by only a metre of quartz-muscovite schist; a unit that only occurs together with the massive sulphides (Vokes, 1963; Skauli, 1990). Shearing and a well developed schistosity defined by white mica and biotite, appear in the outer 5-10 metres of microcline gneiss toward the contact to the massive sulphides. This zone gradually passes in to a more massive variety in the interior part of the gneiss body, where white spots of pure microcline aggregates are a characteristic feature. In the matrix, white microcline, albite, biotite, muscovite and minor amounts of plagioclase and quartz can be identified by the naked eye. Quartzo-feldspatic leucosomes associated with biotite-rich melanosome give the rock its gneissic qualities and lensoid dark xenoliths composed of biotite locally provides it with a patchy appearance. On weathered surfaces, it is possible to identify a subtle centimetre to decimetre scale layering defined by varying amounts of biotite. At closer inspection it appears that they define a

complex system of bands that merges and separates in a braided pattern. The origin of these structures is not unravelled but one possibility is that they are relicts of a metamorphosed veinlet system.

8 PETROGRAPHY

Microcline composes 70-85 volume percent of the rock. It is granoblastic, fine to medium grained, show tartan twinning and occasionally has perthitic exsolutions of albite. The white spots consists of pure microcline exhibiting perfect evolution of triple junction boundaries between the individual crystals. *Plagioclase* is also granoblastic and fine- to medium-grained but rarely exceeds volumetric proportions of 5 %. *Quartz* is abundant in the outer 10 to 15 metres of the contact but is absent or scarce in the interior of the gneiss.

Biotite and *white mica* vary in proportion and textures along profile 1. In the sheared contact zone, both minerals are lepidoblastic defining a strong foliation running parallel to the contact. Gradually, over a distance of 15 to 30 metres, the foliation yields and micas with a random orientation dominates. Two generations of white mica can be identified microscopically, first of which occur as fine- to medium-grained greyish stubby poikiloblastic plates with inclusions of quartz. The second generation is fine-grained, appearing as glass-clear elongated rods free of inclusions. In sections where the micas are lepidoblastic, it is clear that the first generation of white mica define a relict foliation with a high angle to the foliation defined by the second generation of white mica.

Biotite is fine- to medium-grained and strongly pleochroitic with colours varying from pale brown to deep olive green.

Clinozoizite is the dominant accessory mineral, locally composing two percent of the rock. It is fine-grained, sub- to euhedral with a well developed zonarity around a core of allanite and, where included in biotite, is surrounded by a radiogenic halo.

Zircon, which has been used for U/Pb geochronology, is sub- to euhedral, fine-grained and are randomly distributed in all the phases described above. They are normally glass clear, inclusion free and devoid of secondary overgrowth.

Finally, the microcline gneiss contain accessory fine-grained sphene, apatite, calcite and in the proximity to the massive sulphides and along the first 15 metres of profile 1, it also contains some pyrrhotite and minor pyrite.

9 WHOLE ROCK CHEMISTRY

Analytical procedures for the XRF analysis are provided as footnotes in Table 1. Major and minor element analysis were obtained at the Laboratory division, the Geological Survey of Norway.

Although the microcline gneiss was exposed to Caledonian metamorphism it is consistently plotting in the trachytic/syenitic field in the (SiO_2) - $(\text{K}_2\text{O}-\text{Na}_2\text{O})$ discrimination diagram (Fig. 2a). This is also so when the $(\text{Zr}/\text{TiO}_2 \cdot 0.0001)$ - (SiO_2) diagram (Fig. 2b) is employed as long as samples from the sheared and altered contact zone of the microcline gneiss are avoided. Consequently, the microcline gneiss are relatively enriched in alkalis and zirconium with average contents of 11.2 weight % and 414 ppm, respectively (Table 1). With an average alkalinity index, $(\text{Na}_2\text{O}+\text{K}_2\text{O}):\text{Al}_2\text{O}_3 \approx 1$, and with the ratio $\text{SiO}_2:6(\text{Na}_2\text{O}+\text{K}_2\text{O}) \leq 0.6$, the

microcline gneiss will classify as an alkaline syenite of miaskitic to agpaitic composition. Elements that normally are hydrothermally immobile, including TiO_2 , Al_2O_3 , Zr and Ba, follow a falling trend when plotted against SiO_2 in Harker variation diagrams. TiO_2 and Al_2O_3 show a strong positive correlation with Zr and follow a trend intercepting at the origin of the diagram (Fig. 2g and 2h). They can therefore be regarded as conserved elements with little or no post-magmatic redistribution. When the conserved elements are plotted as a function of the distance along profile 1, they follow a smooth weakly falling trend from the contact in to the interior of the microcline gneiss (Fig. 3a-c). This is in contrast to Fe_2O_3 , MgO and the alkalis that show strong fluctuations in the first 30 metres of profile 1, after which they remain constant for the remaining part of the profile. The nature of the processes that were responsible for the apparent disturbance in the distribution of Fe, Mg and the alkalis, can be evaluated with Pearce Element Ratio analyses (PER-analysis). This approach is addressing the changes seen in a magmatic rock undergoing post-magmatic alteration (Pearce, 1968; Stanley and Madeisky, 1993, 1994; Madeisky, 1995).

The basis for this technique is that the ratio between any magmatic element and a conserved denominator constituent (the PER-denominator) is employed. Zirconium, for example, normally approach incompatible and immobile behaviour during magmatic processes and post magmatic hydrothermal alteration. When one element ratio is plotted against another element ratio with the same PER-denominator the samples will follow a linear trend, or fall in a narrow cluster. Any deviation from a linear relationship or a cluster, will normally be a function of post-magmatic mass transfer, where one or both of the numerator elements were added or leached relative to the original system.

Zirconium, showing almost perfect incompatible and immobile behaviour, is chosen as the PER-denominator element in Fig. 4. In the first five diagrams (Fig. 4a-e) the relevant elements are plotted against $1/\text{Zr}$ to test if they were added, subtracted or remained constant after crystallisation of the microcline gneiss. Silica and Al follow a smooth line (Fig. 4a) and, therefore, maintained constant proportions during alteration of the microcline gneiss. The whole rock samples from the first 30 metres of profile 1 show evidence of extensive remobilisation of the alkalis, Ca, Fe and Mg (Fig. 4b-e). Apparently, the microcline gneiss is depleted in the alkalis and Ca in the first 30 metres because the samples plot below the line through the unaltered samples from profile 1, whereas Fe and Mg, plotting above the line, are added to the system. The behaviour of the alkalis + Ca are tested in Fig. 4f. Unaltered samples should plot along a line defining the trend for an unaltered igneous rock where Ca, Na and K primarily will fractionate in favour of plagioclase, orthoclase or biotite. From this figure, it is clear that the outer 30 metres of the microcline gneiss has suffered alkali depletion. However, alkali depletion does not continue beyond the stability limit of muscovite (e.g. forming chlorite), because all the samples plot above the line defining a rock where all the alkalis are fixed by muscovite.

10 EMP-ANALYSIS

EMP analysis were conducted at the Continental Shelf Institute, Norway. Analytical procedures are given in footnotes to Table 2.

From the petrographic studies it became clear that biotite and white mica are the only phases that can accommodate the amount of Mg and Fe reported from the whole rock XRF-analysis. EMP analysis of these minerals should, therefore, shed light over the distribution of Fe and Mg as it is seen along profile 1 and in the PER-analysis.

The composition of the biotites change gradually from phlogopites with a Mg/Fe molar ratio of 3.8 adjacent to the Bleikvassli ore deposit, to more iron-rich compositions with a ratio of 0.35 at 30 metres, after which the Mg/Fe ratio remain fairly constant at 0.3 throughout the rest of profile 1 (Table 2, Fig. 5a). Parallel with this progressive iron-enrichment, the total concentration of fluorine in biotite decreases from 1.4 % in the proximity to the massive sulphides, to a constant level of 0.2 % at 30 metres and for the rest of profile (Fig. 5b).

Due to their relatively high contents of FeO, MgO and SiO₂, the white micas can be classified as phengites (Table 2). Similar to the biotites, they show a gradual decrease of the MgO concentration up to 30 metres away from the massive sulphides after which they maintain a constant level (Fig. 5c). They also show a gradual decrease in the Al₂O₃ component (Fig. 5d) but fail to show a systematic relationship of the F and FeO with distance.

11 GEOCHRONOLOGY

Samples for U/Pb geochronology were obtained from the unaltered interior of the microcline gneiss and a zircon concentrate was separated using standard heavy liquid and magnetic techniques. The zircon concentrate was cleaned in successive solutions of 7 N HNO₃ and 6 N HCL and distilled water to remove contaminant sulphides and surface impurities. Following this procedure, the zircons were split according to their magnetic character using a Frantz Isodynamic Barrier separator and, finally, sieved to provide populations of desired size range and magnetic character. Representative samples were hand picked to purity, and two of the fractions were air abraded in a device similar to that described by Krogh (1982). Zircon dissolution and ion-exchange procedures were comparable to those described by Krogh (1973) and Parish and others (1987). A mixed ²⁰⁵Pb-²³³U-²³⁵U tracer was employed. Lead and uranium were loaded on Tungsten and Rhenium filaments and analysed on the Finnigan MAT 261 multi collector mass spectrometer at Brown University. Lead was analysed in static multi collector mode employing Faraday cup collection of masses 208, 207, 206 and 205 while simultaneously collecting mass 204 in a secondary electron multiplier. Uranium was analysed in static multi collector mode employing Faraday cup collectors only. Additional analytical data are given in the footnotes to Table 3.

Although four fractions were processed only three were successfully analysed. The data are shown in Table 3 and are graphically displayed on Figure 7. For all three analysed fractions, U-Pb systematics are simple and normally discordant. A chord constructed through the data points has an upper intercept of 481 ±2 Ma whereas the lower concordia intercept is essentially 0 Ma. No geologic significance is attached to the lower concordia intercept. The well-constrained upper intercept of 481 ±2 Ma is interpreted as the cooling age of the syenitic protholith to microcline gneiss.

12 DISCUSSION

Origin of the microcline gneiss

In a previous study of the microcline gneiss, it was suggested that this body represents the metamorphosed equivalent of a potassic alteration zone formed in a pelitic sedimentary protholith, simultaneously with the genesis of the Bleikvassli ore-deposit (Skauli, 1993). Although we can confirm many of the observations put forward in the study of Skauli, it is clear that a syn-genetic relationship between the massive sulphides and the genesis of the microcline gneiss protholith does not concur with our results. Accordingly, our data imply that the microcline gneiss represents a metamorphosed alkaline igneous rock of syenitic composition that intruded at 481 ±2 Ma. Secondary metamorphic overgrowth on the zircons

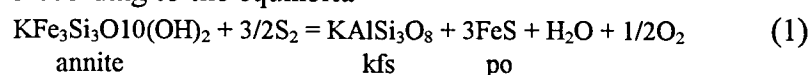
was not observed during the microscopic studies, and the fact that both abraded and unabraded fractions give the same age indicate that the zircons were not influenced by metamorphism. Being a syn-sedimentary SEDEX deposit (Skauli, 1990, 1992, 1993), the Bleikvassli occurrence must have an age close to the age of sedimentation at 590-600 Ma, as indicated by $^{87}\text{Sr}/^{86}\text{Sr}$ analyses of dolomite and calcite marbles or definitely be older than 576 ± 7 Ma which is the minimum age of the meta-sediments (Marker, 1983; Senior and Andriessen, 1990). Being >100 Ma older than the microcline gneiss, a genetic relationship between this rock and the massive sulphides seems inconceivable. Furthermore, the well constrained linear correlation of conserved elements is difficult to obtain in a sedimentary rock, whereas these trends are quite common in igneous rocks. Also the linear correlation, of unaltered microcline gneiss, along the feldspar line in Fig. 4f supports a magmatic origin of this rock. Much more scatter of the analysed samples would be expected if this rock had a sedimentary origin. Finally, diamond drilling in the vicinity of the Bleikvassli deposit (*pers. com.* Olav Bakke) and mapping elsewhere in the region, have revealed four other bodies of microcline gneiss, none of which are related to massive sulphide deposits (Bjerkgård et al, *in prep*).

Excluding the altered samples along the first 30 metres of profile 1, the microcline gneiss show a remarkably high K_2O concentration yielding an average of 8.57 %. Igneous rocks with this much potassium are limited in abundance but has been described from numerous localities around the world (Table 1). Therefore they are not unique as stated elsewhere (Skauli, 1993). Some recently published examples would include the Barrel Spring pluton in USA (Gleason et al., 1994), the Salmi pluton in Russia (Sviridenko, 1994), the Degana pluton in India (Chattopadhyay, 1994), some syenites and K-phonolites from China (Yu et al., 1994) and many potassic and ultra potassic rocks (see review by Pecerillo, 1992).

Alteration of the microcline gneiss

Although alteration of the microcline gneiss did not occur during the genesis of the Bleikvassli deposit, the first 30 metres along profile 1 did suffer significant metasomatism when the microcline gneiss was metamorphosed together with the massive sulphides. As indicated by the PER analysis, K, Na and Ca were leached in a 30 metres wide zone, whereas Fe and Mg were added to the system. The exact nature of metasomatism is difficult to conceive although a qualitative approach explaining the behaviour of Fe and Mg can be obtained. Figure 6 illustrates the almost perfectly negative correlation between F and the concentration of Fe in the biotites. This effect, known as F-Fe avoidance, bear on the principle that biotites with a high Mg/Fe ratio can incorporate more F in their crystal lattice than biotites with lower Mg/Fe ratios (e.g. Munoz, 1984; Kullerud, 1995). Although the ionic radii for F and OH are almost identical and perfect substitution between these two elements are expected, NMR studies documents that F specifically avoid substitution with OH at sites where this component is coordinated with Fe^{2+} (Sanz and Stone, 1979). As a consequence, high concentrations of F in biotites from the microcline gneiss requires the decomposition of iron-rich biotites constituting the unaltered part of the gneiss body.

Decomposition of iron-rich biotite has been observed in the host rock accommodating the Ducktown massive sulphide deposit (Nesbitt, 1982). Biotite breakdown coincided with amphibolite facies metamorphism as a result of the high sulphur fugacity of the system. According to the equilibria

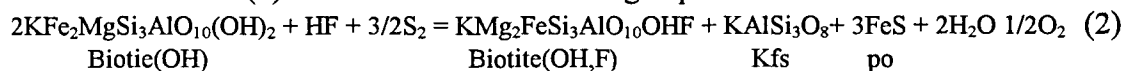


the decomposition of annite includes the formation of K-feldspar, H_2O and pyrrhotite.

Recent studies document that metamorphosis of the Bleikvassli deposit indeed imposed a secondary sulphidation-oxidation halo in the hanging wall lithology (Spry et al., 1995). Spry

and co-workers showed that the modal proportions as well as the composition of oxides, sulphides and ferro-magnesian silicates changed systematically as a function of the distance from the Bleikvassli deposit. Important for the present study, is that the mole fraction of Fe (X_{Fe}) in biotite changed from 0.45 150 metres away, to 0.06 at the contact with the massive sulphides.

If reaction (1) is modified to the following expression:



it is more in agreement with the mineralogy observed in the altered part of the microcline gneiss since the formation of F-rich and Mg-rich biotite are included in the equilibria. This reaction path is also indicated on Figure 8 (from Nesbitt, 1982) where biotite must contain progressively more magnesium to remain stable as the f_{S_2} is raised. The shaded field shown on Figure 8 constrain the evolution of biotites along profile 1 in the microcline gneiss. Reaction (2) presume the incorporation of alkalis in feldspar although, as documented previously, the total concentration of alkalis decreases as the massive sulphides are approached (Fig. 4f & 5f). Some of the alkalis were probably dissolved in the metasomatising fluids and removed from the system leaving excess Al_2O_3 and SiO_2 in the altered gneiss. SiO_2 could conveniently be incorporated in quartz in agreement with the higher proportions of this phase seen in the altered part of the microcline gneiss. Excess Al_2O_3 can be accommodated by phengite because this phase show a 5-7 % increase in Al_2O_3 , as the Bleikvassli ore-deposit is approached.

13 APPLICATION TO EXPLORATION

Nesbitt (1982) and Spry et al. (1995) launched the idea that the sulphidation-oxidation halo surrounding metamorphosed massive sulphide occurrences can be used as an exploration target. Agreeing with this point of view, we would suggest that prospecting for fluorine as well, could be worth the effort because the concentration of this element in biotite is so closely correlated with the presence of a sulphidation-oxidation halo. If fluorine was added to the host rock during metamorphism of the massive sulphide, rather than just being the result of local diffusion from e.g. apatite into biotite, simple whole rock trace element analysis of fluorine could be sufficient to reveal the existence of a sulphidation-oxidation halo. This approach would be less expensive and labour intensive compared with the otherwise necessary microprobe analysis which are a prerequisite for the determination of Fe/Mg ratios in the ferro-magnesian silicates. Some EMP analyses of biotites will, however, be imperative to document if enhanced fluorine concentrations is an effect of sulphidation-oxidation phenomena or is the result of processes unrelated to massive sulphide occurrences. These investigations could be combined with PER analysis as long as the host rocks have a relatively uniform composition and/or, has a magmatic origin. In this context, it is important to note that the analysis of fluorine in biotite is independent of the origin of the protholith and, therefore, can be applied to regions with a complex igneous and sedimentary lithology. At present we are testing both approaches on a promising anomaly in the area.

14 CONCLUSION

- * The microcline gneiss in the Bleikvassli area is an intrusive magmatic rock with an alkaline syenitic composition which crystallised at 481 ± 2 Ma. This is >90 Ma later than deposition of the meta-sedimentary host rock and the genesis of the Bleikvassli ore-deposit.
- * During Caledonian metamorphism, a 30 metres wide zone adjacent to the massive sulphide deposit underwent extensive metasomatic alteration involving the depletion of K, Na and Ca and the addition of Fe and Mg.
- * Sulphidation-oxidation reactions associated with metamorphosis of the massive sulphides, provoked the decomposition of iron-rich biotites in the proximity to the ore-deposit and the formation of Mg-rich biotites and more aluminous white mica compared to the unaltered parts of the microcline gneiss.
- * Formation of Mg-rich biotites greatly enhanced the incorporation of fluorine in this mineral. The fluorine was probably added from the hydrothermal fluids that altered the microcline gneiss.
- * Because the incorporation of fluorine in the biotites is a direct effect of the presence of a sulphidation-oxidation halo around a massive sulphide deposit, it is possible that the exploration after fluorine anomalies would assist in the discovery of unexposed massive sulphide deposits as long as it can be documented that the fluorine is fixed by biotite.

15 ACKNOWLEDGEMENT

Harald Hatling, Geological Survey of Norway, conducted the initial sample preparation and heavy liquid separation of zircons for U/Pb dating and the Laboratory division, Geological Survey of Norway, obtained the XRF analysis. Microprobe analysis were done at the Norwegian Continental Shelf Institute under the supervision of Tony Boassen. This project was partially funded by Hemnes Municipality, Nordland County and the mining company, Bleikvassli Gruber. Tor Grenne reviewed an earlier draft of this manuscript.

16 REFERENCES

- Chattopadhyay B., Chattopadhyay S., and Bapna V. S. (1994) geology and geochemistry of the Degana pluton - a proterozoic rapakivi granite in Rajasthan, India. *Mineral. Petrol.* **50**, 69-82.
- Cook N. J. (1993) Conditions of metamorphism estimated from alteration lithologies and ore at the Bleikvassli Zn-Pb-(Cu) deposit, Nordland, Norway. *Norsk Geologisk Tidsskrift* **73**, 226-233.
- Gleason J. D., Miller C. F., Wooden J. L., and Bennet V. C. (1994) Petrogenesis of the highly potassic 1.42 Ga Barrel Spring pluton, south-eastern California, with implications for mid-Proterozoic magma genesis in the south-western USA. *Contrib. Min. Petrol.* **118**, 182-197.
- Hansen T. S. (1985) The geological evolution of Rostafjell (in Danish). M.S. dissertation, Univ of Copenhagen.
- Krogh T. E. (1973) A low contamination method for hydrothermal decomposition of zircon and extraction of U and Pb for isotopic age determination. *Geochim. Cosmochim. Acta* **37**, 485-494.
- Krogh T. E. (1982) Improved accuracy of U-Pb ages by the creation of more concordant systems using an air abrasion technique. *Geochim Cosmochim Acta* **46**, 560-567.
- Kullerud K. (1995) Chlorine, titanium and barium-rich biotites: factors controlling biotite composition and the implications for garnet-biotite geothermometry. *Contrib. Min. Petrol.* **120**, 42-59.
- Larsen P. H. (1984) Simafjell: a structural and petrographic analyses of the central Caledonides, north Norway (in Danish). M.S. dissertation, Univ. of Copenhagen.
- Madeisky H. E. (1995) Quantitative analysis of hydrothermal alteration: application in litho geochemical exploration. Ph.D. dissertation, Imperial College, London.
- Marker M. (1983) Caledonian and pre-Caledonian geology of the Mofjell area, Nordland, Norway. Ph.D. dissertation, Univ. of Copenhagen.
- Munoz J. L. (1984) F-OH and Cl-OH exchange in micas with applications to hydrothermal ore deposits. in *Micas, reviews in mineralogy* (ed. S. W. Bailey), vol. 13, pp. 469-494. Mineralogical Soc. Am.
- Nesbitt B. E. (1982) Metamorphic sulfide-silicate equilibria in the massive sulfide deposits at Ducktown, Tennessee. *Econ. Geol.* **77**, 364-378.
- Olsen S. B. (1984) Kongsfjellet: a structural and metamorphic analysis of the southern part of the Røddingsfjell nappe, Norway (in Danish). M.S. dissertation, Univ. of Copenhagen.

- Parrish R. R., Roddick J. C., Loveridge W. D., and Sullivan, R. W. (1987) Uranium lead analytical techniques at the geochronology laboratory. *Geological Survey of Canada Paper* **87/2**, 3-7
- Pearce T. H. (1968) A contribution to the theory of variation diagrams. *Contrib. Min. Petrol.* **19**, 142-157.
- Pecerillo A. (1992) Potassic and ultrapotassic rocks: Compositional characteristics, petrogenesis, and geologic significance. *Episodes* **15/4**, 243-251.
- Ramberg I. B. (1967) The geology of the Kongsfjell area: a petrographic and structural investigation in Helgeland, north Norway (in Norwegian, English summary). *Bull. Geological Survey of Norway* **240**, 1-147.
- Rasmussen F. O. (1984) The Reinfjell - Plura area, a part of a double folded duplex structure (in Danish). M.S. dissertation, Univ. of Copenhagen.
- Sanz J., and Stone W. E. E. (1979) NMR studies of micas. II. Distribution of Fe²⁺, F⁻ and OH⁻ in the octahedral sheet of phlogopite. *Am. Mineral.* **64**, 119-126.
- Senior A., and Andriessen P. A. M. (1990) U/Pb and K/Ar determinations in the Upper and Uppermost Allochthons, central Scandinavian Caledonides. *Geonytt* **1/90**, 99 (abstr.).
- Skauli H. (1990) The Bleikvassli zinc-lead deposit, Nordland Norway; petrography, geochemistry and depositional environment. *Interne Skrifter Institute of Geology, Univ. Oslo*, 355 pp.
- Skauli H. (1993) A metamorphosed potassic alteration zone associated with the Bleikvassli Zn-Pb-Cu orebody, northern Norway. *Lithos* **31**, 1-15.
- Skauli H., Bjørlykke A., and Thorpe R. I. (1992a) The bleikvassli lead-zinc deposit, Nordland Norway; lead isotopes of the ore and the alteration zone. *Mineral. Deposita* **27**, 276-283.
- Skauli H., Boyce A. J., and Fallick A. E. (1992b) A sulphur isotope study of the Bleikvassli zinc-lead deposit, Nordland, northern Norway. *Mineral. Deposita* **27**, 284-292.
- Spry P. G., Rosenberg J. L., Jacobson C. E., and Vokes F. M. (1995) A metamorphic sulfidation-oxidation halo associated with the Bleikvassli Zn-Pb-(Cu) deposit, Nordland, Norway. *Proc. of the 3rd biennial SGA meeting, Prague/Czech Republic*, 909-912.
- Stacey J. S., and Kramers J. D. (1975) Approximation of terrestrial Pb isotope evolution by a two-stage model. *Earth and Planet. Sci. Lett* **26**, 207-221.
- Stanley C. R., and Madeisky H. E. (1994) Litho geochemical exploration for metasomatic zones associated with hydrothermal ore deposits using Pearce element ratio analysis. In *Alteration and alteration processes associated with ore-forming systems* (ed. D. R. Lentz), Short Course Notes, vol. 11, pp. 193-211. Geological Association of Canada

- Stephens M. B., Gustavson M., Rambegr I. B., and Zachrison E. (1985) The Caledonides of north-central Scandinavia - a tectonostratigraphic overview. in *the Caledonide orogen - Scandinavia and related areas* (eds. D. G. Gee and B. A. Sturt), pp. 135-162. Wiley.
- Sviridenko L. P. (1994) the evolution of the fluid phase during the crystallisation of granite types: Salmi Pluton, Karelia, Russia. *Mineral. Petrol.* **50**, 59-67.
- Trønnes R. G., and Sundvoll B. (1995) Isotopic composition, deposition ages and environments of Central Norwegian Caledonian marbles. *Bull. Geological Survey of Norway* **427**, 44-47.
- Vokes F. M. (1963) Geological studies on the Caledonian pyritic zinc-lead orebody at Bleikvassli, Nordland, Norway. *Bull. Geological Survey of Norway* **222**, 1-126
- Vokes F. M. (1966) On the possible modes of origin of the Caledonian sulfide ore deposit at Bleikvassli, Nordland, Norway. *Econ. Geol.* **61**, 1130-1139.
- Vokes F. M. (1976) Caledonian massive sulphide deposits in Scandinavia: a comparative review. in *Handbook of strata-bound and stratiform ore deposits* (ed. K. H. Wolf), Vol. 6, pp. 79-123.
- Yu J., Fu H., Zhang F., and Wan F. (1994) Petrogenesis of potassic alkaline volcanics associated with rapakivi granites in the Proterozoic rift of Beijing, China. *Mineral. Petrol.* **50**, 83-96.

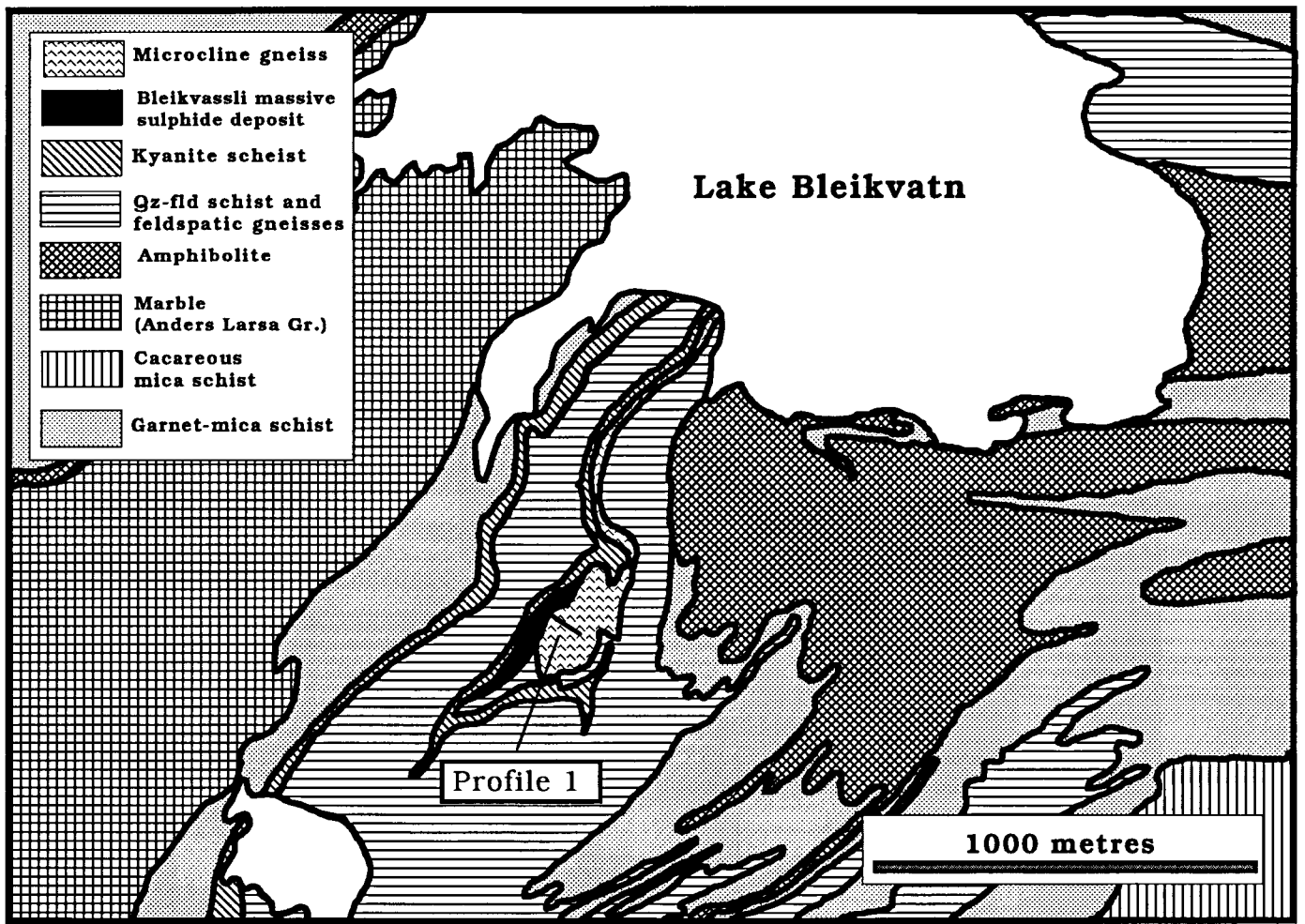


Figure 1

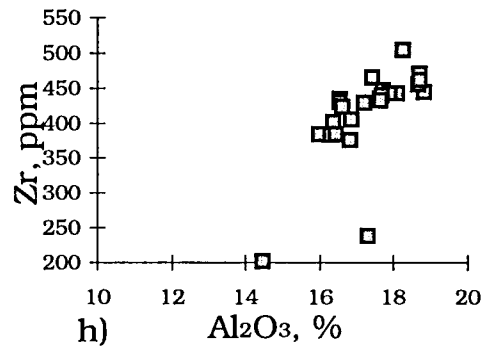
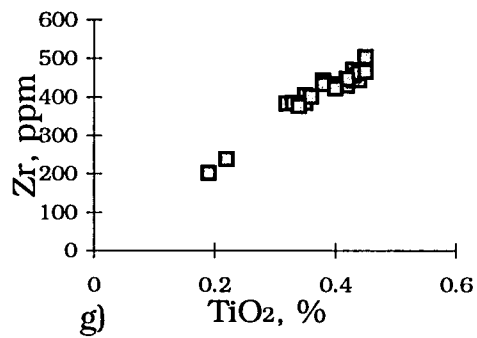
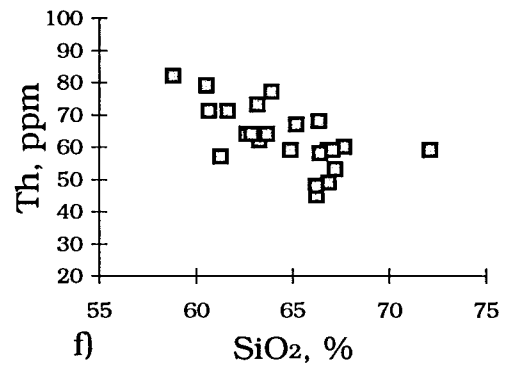
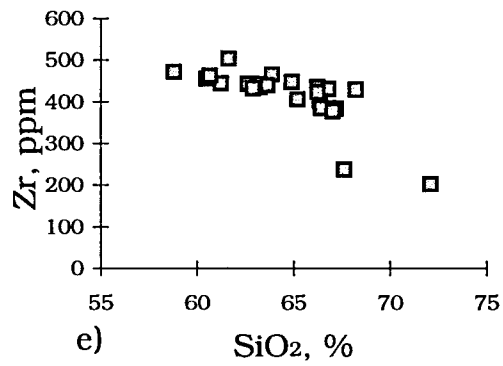
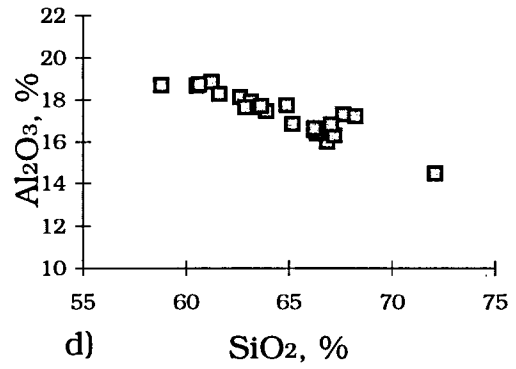
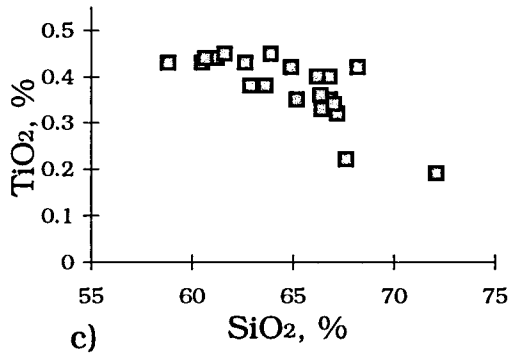
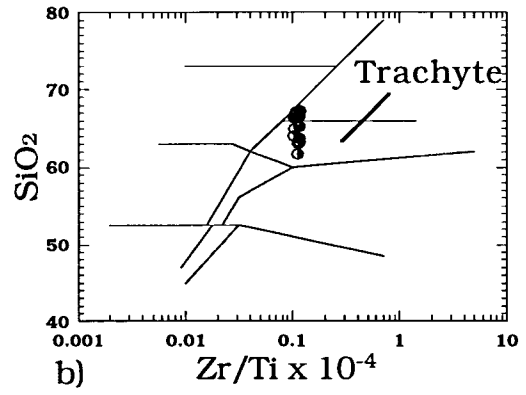
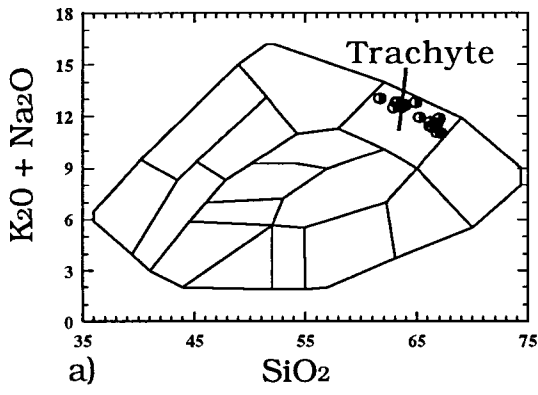


Figure 2

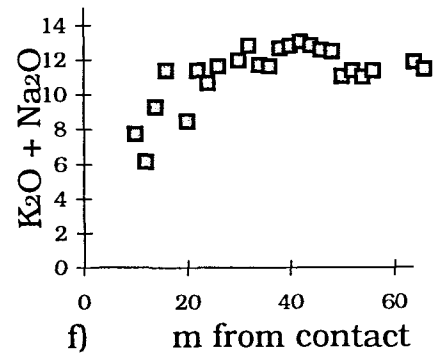
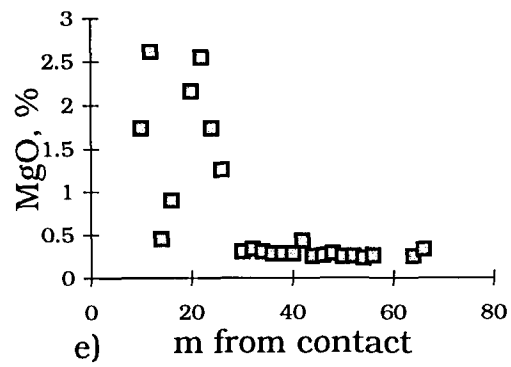
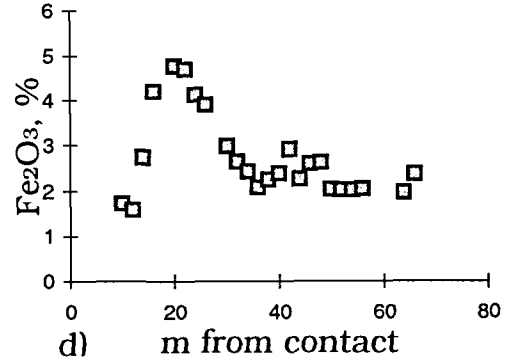
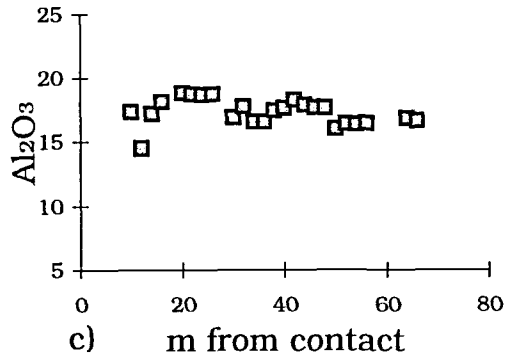
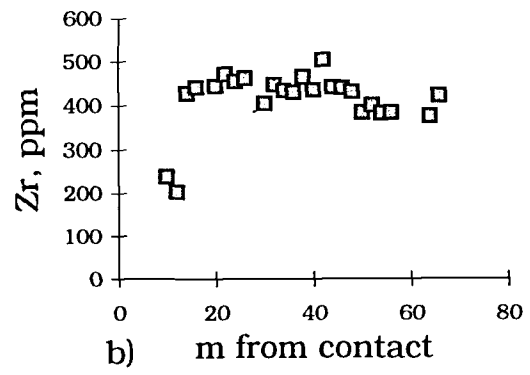
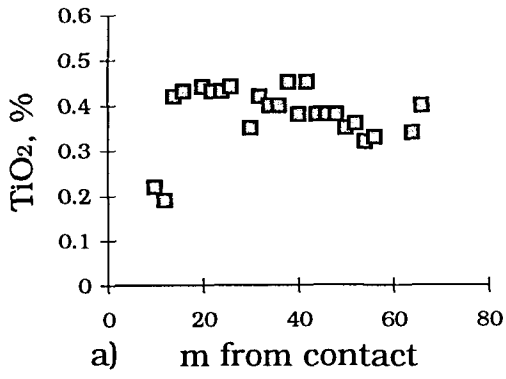


Figure 3

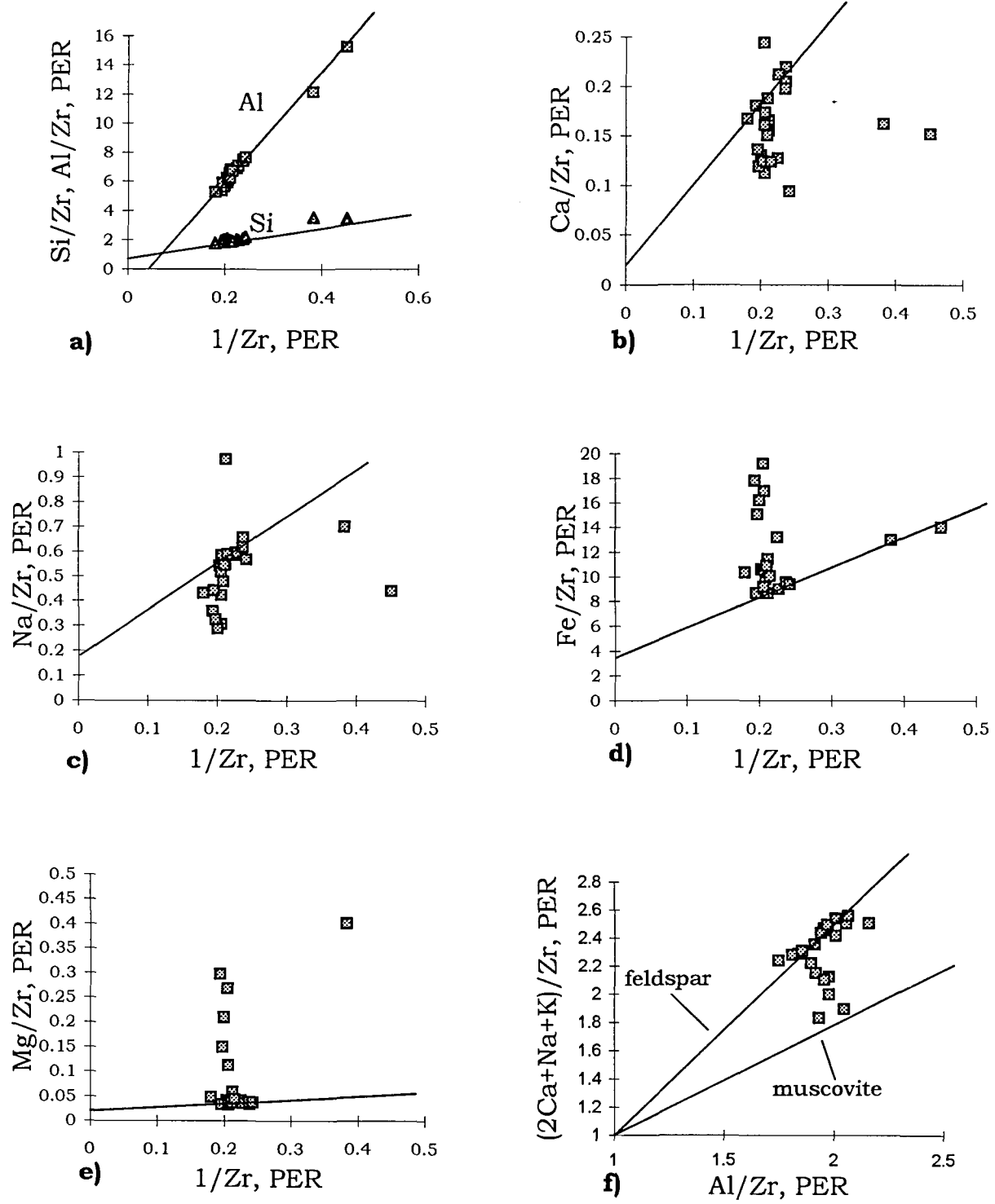


Figure 4

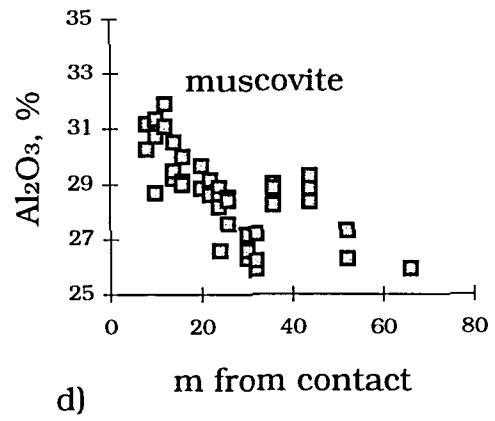
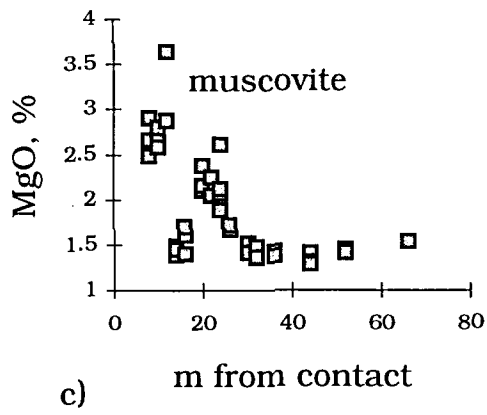
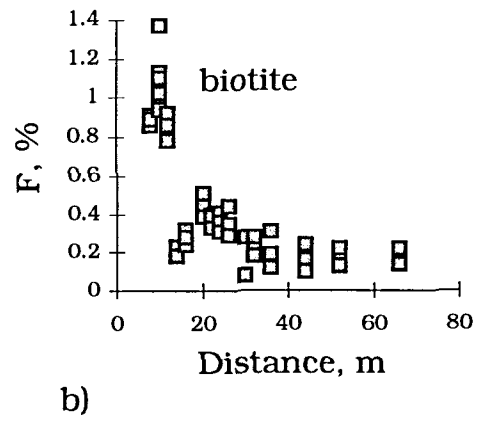
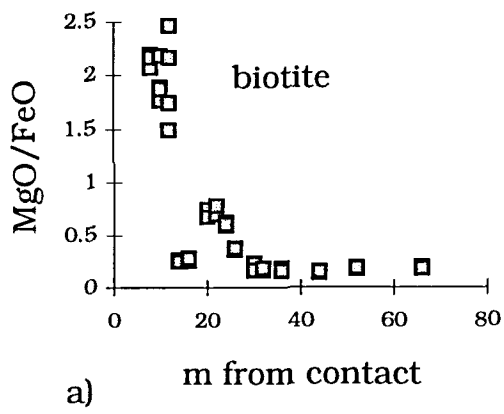


Figure 5

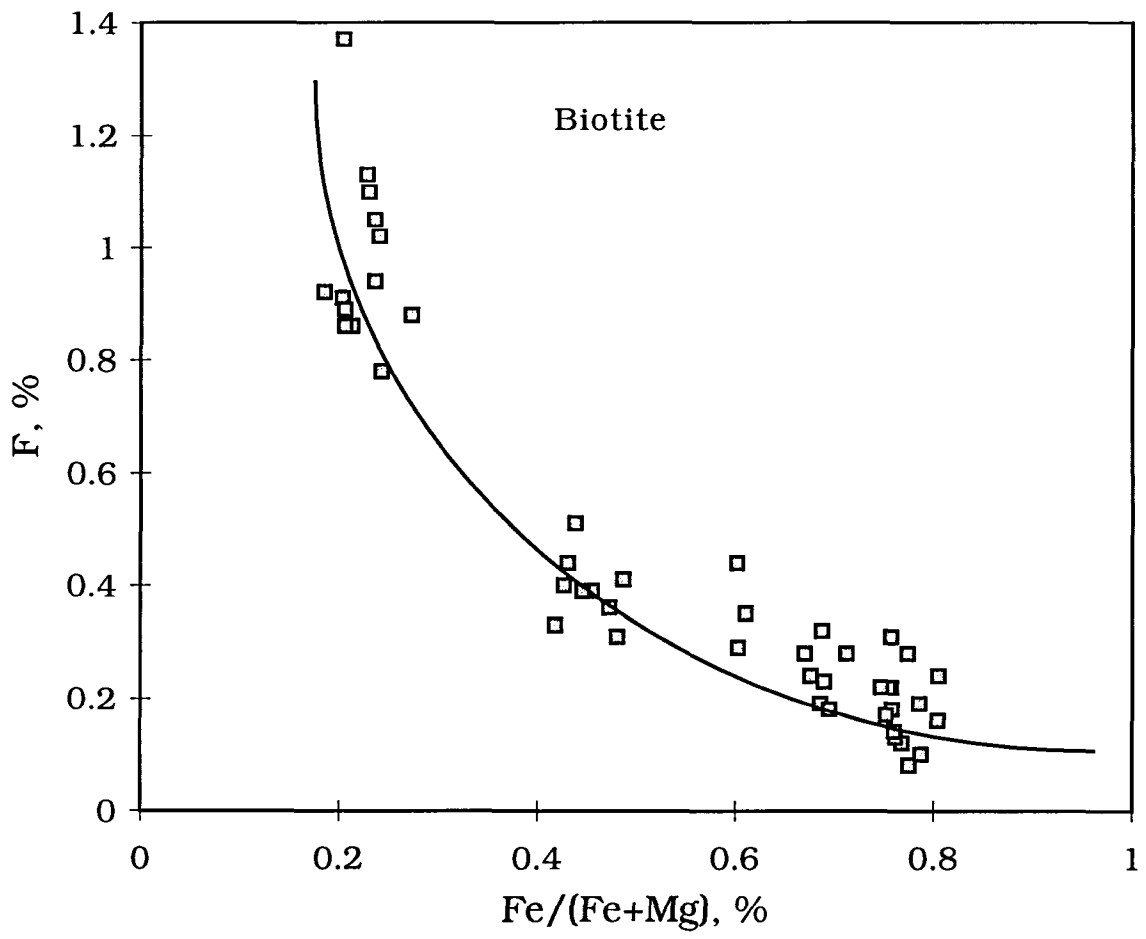


Figure 6

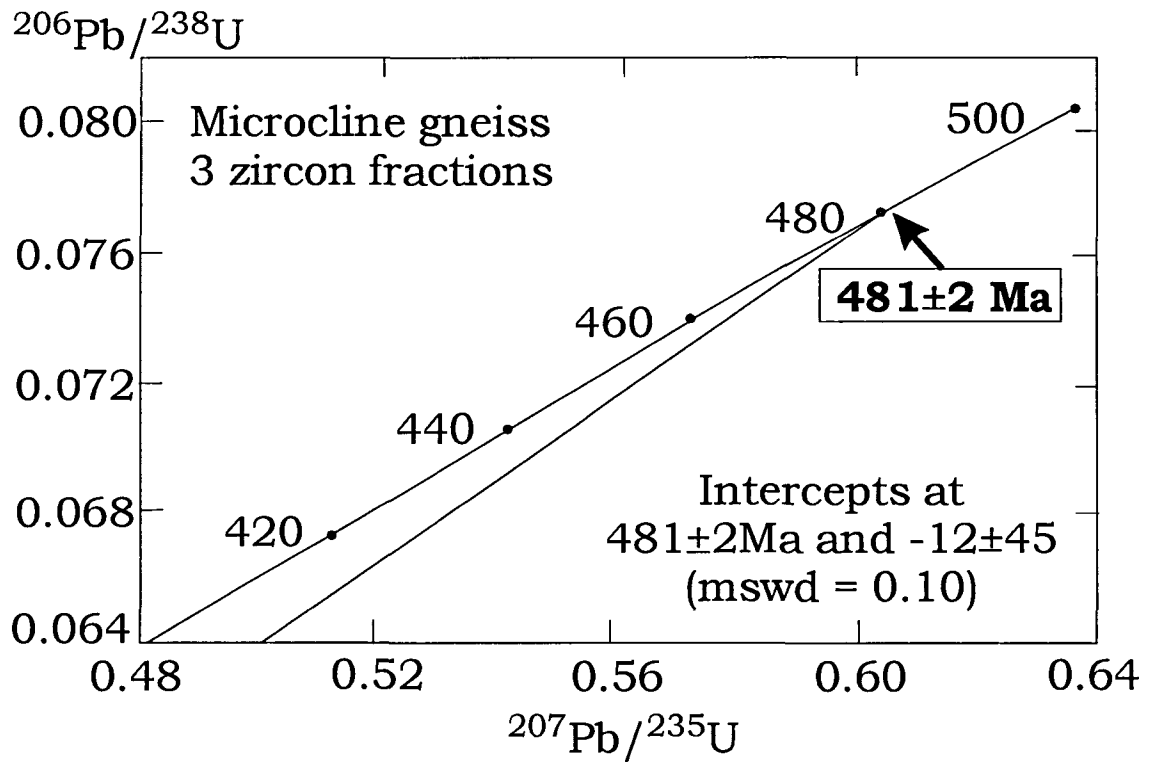


Figure 7

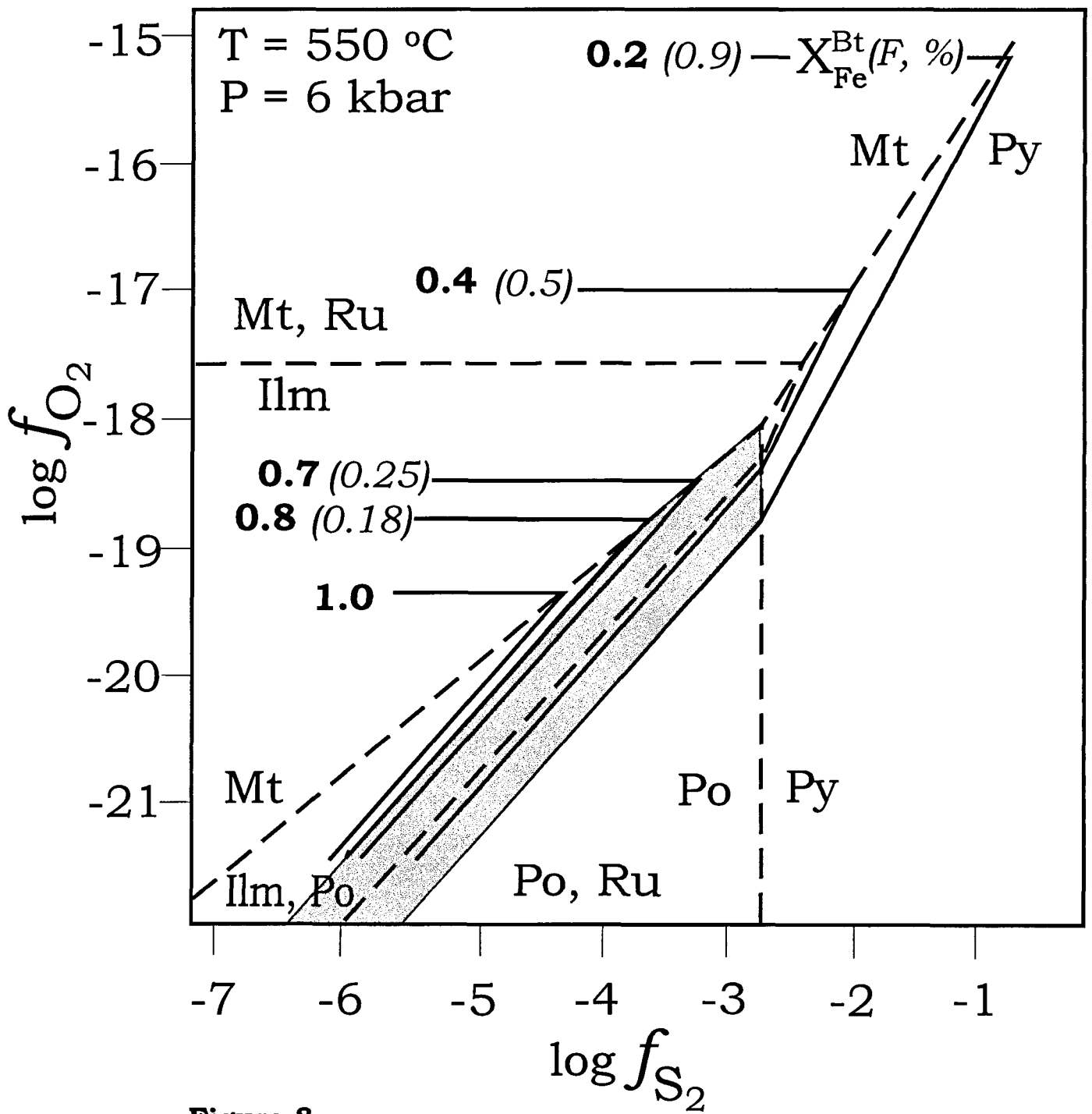


Figure 8

Table 1: XRF analysis

Sample	94022 ¹	94019 ¹	94017 ¹	94007 ¹	94008 ¹	Degana ²	Beijing ³	Barrel ⁴
m from ore	48	42	38	14	16			
<i>Major elements (weight percent)⁵</i>								
SiO ₂	62.88	61.63	63.9	68.22	62.63	63.95	60.38	61.82
Al ₂ O ₃	17.64	18.26	17.43	17.19	18.1	19.39	17.08	15.35
Fe ₂ O ₃ [†]	2.63	2.92	2.25	2.75	4.2	0.4	5.69	6.01
TiO ₂	0.38	0.45	0.45	0.42	0.43	0.02	0.33	1.07
MgO	0.28	0.43	0.28	0.45	0.9	0.1	0.55	1.26
CaO	1.24	1.29	0.97	1.02	0.76	0.32	0.21	1.26
Na ₂ O	3.47	3.2	3.03	6.15	2.76	4.7	1.74	2.95
K ₂ O	8.99	9.81	9.62	3.11	8.61	9.2	11.96	8.48
MnO	0.02	0.02	0.02	0.02	0.02	0.01	0.13	0.06
P ₂ O ₅	0.16	0.19	0.18	0.14	0.17	0.03	0.07	0.3
Gl.tap	0.68	0.4	0.31	0.57	0.91	1.07	1.45	0.91
Total	98.37	98.61	98.45	100.03	99.48	99.19	99.59	99.47
<i>CIPW norm</i>								
Q	7.56	2.6	5.76	18.19	11.24	0.68	3.44	8.72
or	57.99	59.09	54.43	18.49	51.66	55.46	72.08	50.89
ab	26.1	27.54	30.02	52.25	23.66	40.48	14.98	25.3
an	3.83	5.38	5.34	4.26	2.81	1.44	0.64	3.58
lc	0	0	0	0	0	0	0	0
ne	0	0	0	0	0	0	0	0
C	0.64	0.42	0.27	2.15	3.24	1.18	1.03	0
wo	0	0	0	0	0	0	0	0.41
en	0	0	0	0	0	0	0	0.35
en	0.71	1.09	0.72	1.13	2.28	0.25	1.4	2.84
mt	0.07	0.07	0.07	0.07	0.07	0.03	0.43	0.2
he	2.25	2.93	2.65	2.72	4.21	0.38	5.5	5.96
ap	0.4	0.42	0.36	0.31	0.38	0.07	0.16	0.66
sum	99.54	99.54	99.61	99.58	99.56	99.98	99.67	98.92
<i>Minor elements (ppm)⁴</i>								
Nb	22	26	27	26	26	70	50	155
Zr	432	504	465	429	442	50	1202	772
Y	42	54	38	42	39	70	62	67
Sr	165	205	169	199	206	nd	787	24.3
Rb	279	308	280	94	211	nd	318	227
U	<10	11	<10	<10	<10	nd	10.2	nd
Th	263	292	225	275	420	28	120	17
Pb	38	45	45	42	43	nd	nd	nd
V	28	43	28	45	90	nd	138	1.5
As	<10	<10	<10	16	29	nd	nd	nd
Sc	<10	11	<10	<10	<10	3.9	10.8	nd
Ba	542	617	645	250	564	50	2438	206
Ga	17	21	16	16	21	nd	nd	30
Zn	46	80	41	67	69	60	133	nd
Ni	<5	<5	<5	15	16	nd	9	4
Ce	203	219	209	238	239	83	599	219
La	144	170	161	131	175	45	332	111
Nd	123	145	142	81	129	nd	215	105

¹) Microcline gneiss; ²) Chattopadhyay et al. (1994); ³) Yu et al. (1994); ⁴) Glaeson et al. (1994); ⁵) Major element values obtained by XRF on fused glass discs whereas minor element numbers were obtained by XRF analysis on pressed powder tablets. Samples 94017, 94019 and 94022 are representative for the unaltered microcline gneiss; samples 94014 and 94016 are representative for the altered microcline gneiss.

Table 2: EMPA analysis

	Biotite						Muscovite					
Sample	94004	94010	94011	94014	94016	94020	94004	94007	94010	94011	94014	94025
m from ore	8	22	24	32	36	44	8	14	22	24	32	66
Na ₂ O	0.09	0.07	0.04	0.03	0.02	0.04	0.28	0.30	0.29	0.28	0.23	0.17
MgO	18.94	12.73	11.20	4.90	4.54	3.87	2.68	1.44	2.15	2.17	1.40	1.54
Al ₂ O ₃	15.40	15.47	15.28	15.28	15.76	15.68	33.38	29.73	28.89	28.02	26.43	25.92
SiO ₂	40.49	37.48	36.65	35.62	35.05	35.44	48.12	49.21	48.98	47.72	46.95	49.25
K ₂ O	10.61	9.51	10.13	9.39	9.26	9.38	9.38	9.02	8.34	10.01	10.13	10.33
TiO ₂	1.02	2.21	2.30	2.55	2.76	2.69	0.41	1.13	1.27	0.93	0.91	0.90
FeO ¹	8.83	17.15	18.46	28.12	27.11	27.40	1.71	6.00	5.20	5.67	7.68	6.94
F	0.89	0.37	0.36	0.23	0.21	0.17	0.19	0.11	0.05	0.05	0.09	0.14
Cl	0.01	0.01	0.01	0.02	0.03	0.03	0.01	0.00	0.01	0.01	0.01	0.00
Total	96.27	95.00	94.44	96.15	94.74	94.70	96.15	96.94	95.16	94.86	93.84	95.19
O = F+Cl	0.38	0.16	0.15	0.10	0.09	0.08	0.08	0.04	0.02	0.02	0.04	0.06
New total	96.65	95.15	94.59	96.25	94.83	94.78	96.23	96.98	95.18	94.88	93.88	95.25
<i>Number of ions based on 24 (O, OH, F)</i>												
Si ^{II}	6.12	5.94	5.92	5.90	5.86	5.93	6.32	6.53	6.57	6.52	6.57	6.75
Al ^{IV}	1.88	2.06	2.08	2.10	2.14	2.07	1.68	1.47	1.43	1.48	1.43	1.25
Al ^{VI}	0.86	0.83	0.83	0.88	0.97	1.03	3.48	3.17	3.13	3.03	2.93	2.93
Ti	0.12	0.26	0.28	0.32	0.35	0.34	0.04	0.11	0.13	0.10	0.10	0.09
Fe ²⁺	1.12	2.27	2.49	3.89	3.79	3.84	0.19	0.67	0.58	0.65	0.90	0.80
Mg	4.27	3.01	2.70	1.21	1.13	0.97	0.53	0.29	0.43	0.44	0.29	0.32
Na	0.03	0.02	0.01	0.01	0.01	0.01	0.07	0.08	0.08	0.07	0.06	0.05
K	2.05	1.92	2.09	1.98	1.98	2.00	1.57	1.52	1.43	1.75	1.81	1.81
F	0.85	0.37	0.37	0.24	0.22	0.18	0.15	0.09	0.04	0.04	0.08	0.12
Cl	0.01	0.00	0.00	0.01	0.02	0.02	0.00	0.00	0.00	0.00	0.00	0.00
Cations	16.43	16.32	16.40	16.29	16.22	16.19	13.87	13.83	13.77	14.03	14.09	13.99
Oxygen	24.00	24.00	24.00	24.00	24.00	24.00	24.00	24.00	24.00	24.00	24.00	24.00
Mg#	3.82	1.32	1.08	0.31	0.30	0.25	3.59	0.55	0.95	0.88	0.42	0.51
n	3	3	3	3	3	3	3	3	3	3	3	1

¹⁾ All iron as Fe²⁺. Analytical procedure: All elements were analysed on a Jeol Superprobe 733 equipped with Tracor Northern automation and ZAF corrections. Quantitative analyses were obtained with wavelength dispersive spectrometry (WDS) using a 25 kV acceleration voltage and a beam current stabilized at 15 ±0.02 nA. All elements were calibrated against natural standard.

Table 3: U/Pb systematics

Fraction properties	Amount analysed (mg)	Concentration (ppm)		Pb Isotopic composition [#]			Ages and uncertainty ^{**}		
		Pb	U	208/206	207/206	206/204	²⁰⁶ Pb*/ ²³⁸ U	²⁰⁷ Pb*/ ²³⁵ U	²⁰⁷ Pb*/ ²⁰⁶ P
nmI ^o , -150 + 100 μm, ab	0.7	38.6	478	0.1844	0.06000	4 461	467.1 ±1.1	469.6 ±1.6	481.9 ±0.5
nmI ^o , -100 + 75 μm, ab	0.4	28.4	359	0.1758	0.05961	5 097	461.0 ±1.5	464.6 ±1.8	481.4 ±0.7
nmI ^o , -100 + 75 μm, -ab	0.5	53.2	700	0.1918	0.05986	4 697	438.1 ±1.9	445.3 ±2.2	482.2 ±1.4

nm = nonmagnetic, m = magnetic, ab = abraded for 12 hours, ^o = side slope of Frantz Isodynamic Barrier Separator operated with a forward slope of 15° and magnet current of 1.8 amps. Values in μm indicate size range of zircons prior to abrasion.

*) denotes total Pb corrected for common Pb in zircon and laboratory blank Pb. Isotopic composition of common Pb is estimated from Stacey and Kramers (1975) but an uncertainty of ±0.1 is assigned to the 207/204 ratio. Total procedural blanks are ~2 picograms for U and 8-38 picograms for Pb.

#) measured isotopic ratios corrected for mass fractionation of -0.11% per atomic mass unit based on replicate analyses of NIST SRM 981 and 982 and adjusted for small amount of ²⁰⁶Pb in tracer.

**) decay constants: ²³⁸U = 1.5513E-10/yr; ²³⁵U = 9.8485E-10/yr. Atom ratio ²³⁸U/²³⁵U = 137.88. Uncertainty in the calculated ages is stated at the 2σ level and estimated from combined uncertainties in calibrations of mixed ²⁰⁵Pb - ²³³U - ²³⁵U tracer, measurement of isotopic ratios of Pb and U, blank Pb-isotopic ratios, Pb and U mass fractionation corrections and reproducibility in measurement of NIST, Pb and U standards.

Appendix 1: XRF analysis of samples from the microcline gneiss

Sample	94005	94006	94011	94007	94008	94009	94010	94012
m from ore	10	12	14	14	16	20	22	26
<i>Major elements (weight %)</i>								
SiO ₂	67.64	72.11	60.52	68.22	62.63	61.25	58.82	60.66
Al ₂ O ₃	17.3	14.47	18.66	17.19	18.1	18.83	18.7	18.71
Fe ₂ O ₃	1.73	1.59	4.13	2.75	4.2	4.77	4.7	3.9
TiO ₂	0.22	0.19	0.43	0.42	0.43	0.44	0.43	0.44
MgO	1.73	2.61	1.73	0.45	0.9	2.15	2.54	1.25
CaO	0.59	0.47	0.91	1.02	0.76	1.66	1.3	0.84
Na ₂ O	2.46	1.31	1.94	6.15	2.76	2	2.49	2.21
K ₂ O	5.25	4.82	8.69	3.11	8.61	6.46	8.89	9.38
MnO	0	0	0.01	0.02	0.02	0.02	0.02	0.02
P ₂ O ₅	0.05	0.04	0.16	0.14	0.17	0.15	0.16	0.16
LOI	1.82	1.7	1.38	0.57	0.91	1.86	0.96	1.15
Sum	98.79	99.32	98.56	100.03	99.48	99.58	99.02	98.72
<i>Minor elements (ppm)</i>								
Nb	32	29	26	26	26	26	26	24
Zr	238	202	455	429	442	444	471	462
Y	40	11	37	42	39	41	39	40
Sr	76	53	166	199	206	189	226	194
Rb	171	158	161	94	211	143	162	220
U	17	0	0	0	0	17	19	0
Th	173	159	413	275	420	477	470	390
Pb	22	19	43	42	43	44	43	44
V	173	261	173	45	90	215	254	125
As	12	0	12	16	29	11	17	0
Sc	0	0	0	0	0	0	0	0
Ba	278	147	674	250	564	510	739	652
Ga	19	16	19	16	21	20	18	18
Zn	318	184	89	67	69	273	121	97
Cu	0	0	0	0	0	0	29	0
Ni	0	0	14	15	16	6	6	0
Yb	0	0	0	0	0	0	0	0
Ce	166	53	224	238	239	188	208	265
La	94	27	156	131	175	124	145	200
Nd	82	33	125	81	129	85	117	159

Sample	94013	94014	94015	94016	94017	94018	94019	94020
m from ore	30	32	34	36	38	40	42	44
<i>Major elements (weight %)</i>								
SiO ₂	65.2	64.91	66.23	66.81	63.9	63.27	61.63	63.17
Al ₂ O ₃	16.85	17.72	16.54	16.54	17.43	17.63	18.26	17.89
Fe ₂ O ₃	2.99	2.65	2.43	2.08	2.25	2.39	2.92	2.27
TiO ₂	0.35	0.42	0.4	0.4	0.45	0.38	0.45	0.38
MgO	0.3	0.33	0.3	0.28	0.28	0.28	0.43	0.25
CaO	0.79	0.85	1.05	1.09	0.97	1	1.29	1.09
Na ₂ O	3.48	3.57	3.55	3.48	3.03	3.06	3.2	3.37
K ₂ O	8.45	9.23	8.11	8.11	9.62	9.72	9.81	9.43
MnO	0.02	0.02	0.02	0.02	0.02	0.02	0.02	0.02
P ₂ O ₅	0.16	0.17	0.16	0.18	0.18	0.16	0.19	0.15
LOI	0.49	0.32	0.31	0.3	0.31	0.29	0.4	0.4
Sum	99.08	100.19	98.98	99.29	98.45	98.19	98.61	98.43
<i>Minor elements (ppm)</i>								
Nb	21	22	23	23	27	23	26	25
Zr	405	447	434	430	465	435	504	442
Y	35	33	39	34	38	37	54	39
Sr	157	143	158	176	169	170	205	173
Rb	224	251	251	245	280	281	308	277
U	0	0	0	0	0	0	11	0
Th	299	265	243	208	225	239	292	227
Pb	35	42	40	40	45	38	45	38
V	30	33	30	28	28	28	43	25
As	0	0	0	0	0	0	0	0
Sc	0	11	13	0	0	11	11	0
Ba	513	618	515	563	645	619	617	563
Ga	17	15	16	17	16	15	21	16
Zn	88	80	71	35	41	48	80	48
Cu	12	0	0	0	0	7	0	0
Ni	0	15	0	18	0	0	0	18
Yb	0	0	0	0	0	11	0	0
Ce	213	215	194	204	209	189	219	204
La	154	174	139	147	161	145	170	155
Nd	129	139	112	123	142	120	145	133

Sample	94021	94022	94023	94024	94025	94026	94027	94028
m from ore	46	48	50	52	54	56	64	66
<i>Major elements (weight %)</i>								
SiO ₂	63.66	62.88	66.87	66.37	67.2	66.44	67.04	66.23
Al ₂ O ₃	17.69	17.64	15.98	16.37	16.3	16.43	16.82	16.61
Fe ₂ O ₃	2.6	2.63	2.04	2.02	2.02	2.05	1.97	2.38
TiO ₂	0.38	0.38	0.35	0.36	0.32	0.33	0.34	0.4
MgO	0.26	0.28	0.24	0.25	0.23	0.26	0.25	0.33
CaO	1.17	1.24	1.29	1.3	1.2	1.16	0.54	0.8
Na ₂ O	3.79	3.47	3.51	3.51	3.71	3.49	3.14	3.67
K ₂ O	8.74	8.99	7.51	7.83	7.28	7.85	8.7	7.73
MnO	0.02	0.02	0.01	0.02	0.01	0.02	0	0.02
P ₂ O ₅	0.16	0.16	0.13	0.13	0.11	0.12	0.15	0.15
LOI	0.34	0.68	0.7	0.69	0.69	0.75	0.51	0.54
Sum	98.8	98.37	98.62	98.85	99.07	98.89	99.45	98.86
<i>Minor elements (ppm)</i>								
Nb	22	22	22	20	22	24	22	19
Zr	440	432	384	401	383	384	376	423
Y	38	42	34	37	37	36	24	34
Sr	184	165	158	162	151	159	170	194
Rb	282	279	242	255	233	248	251	244
U	0	0	0	14	0	0	0	0
Th	260	263	204	202	202	205	197	238
Pb	38	38	35	36	32	33	34	40
V	26	28	24	25	23	26	25	33
As	0	0	0	0	0	0	0	0
Sc	0	0	11	11	0	0	0	0
Ba	496	542	466	469	430	494	590	628
Ga	17	17	18	15	15	17	18	17
Zn	50	46	42	47	40	37	26	45
Cu	0	0	0	0	0	0	0	0
Ni	0	0	16	12	0	0	0	13
Yb	0	0	0	0	0	14	0	0
Ce	211	203	199	202	200	216	104	217
La	152	144	134	142	141	161	68	167
Nd	129	123	112	116	111	120	69	133

Appendix 2: EMP analysis of Biotite and muscovite

App. 2.1: Biotite analysis (concentrations in weight percent)

Sample	m from ore	Na ₂ O	MgO	Al ₂ O ₃	SiO ₂	K ₂ O	TiO ₂	FeO	F	Cl	Sum
94004	8	0.08	18.34	14.96	40.17	10.86	1.05	8.86	0.86	0.02	95.20
94004	8	0.07	19.20	15.64	40.45	10.58	0.99	8.74	0.91	0.01	96.59
94004	8	0.11	19.27	15.60	40.84	10.38	1.03	8.9	0.89	0.01	97.03
94005	10	0.06	17.15	15.72	39.18	9.99	0.97	9.45	1.05	0.00	93.57
94005	10	0.10	17.68	16.19	37.40	9.44	0.88	9.76	0.94	0.00	92.39
94005	10	0.06	17.25	16.04	38.12	9.89	1.16	9.74	1.02	0.00	93.28
94005	10	0.06	17.85	15.54	38.78	9.86	1.12	9.44	1.13	0.01	93.79
94005	10	0.05	20.03	16.62	0.43	9.66	1.01	9.19	1.37	0.01	58.37
94005	10	0.11	18.19	15.99	37.65	10.28	1.04	9.72	1.10	0.01	94.09
94006	12	0.08	12.82	10.78	38.91	10.22	0.71	8.59	0.88	0.01	83.00
94006	12	0.07	15.00	11.94	41.22	8.75	0.79	8.60	0.78	0.03	87.18
94006	12	0.09	19.43	15.76	40.97	10.36	0.75	7.89	0.92	0.01	96.18
94006	12	0.14	19.30	16.26	40.55	9.79	0.80	8.91	0.86	0.00	96.61
94007	14	0.00	6.30	16.14	36.39	9.82	3.62	24.47	0.19	0.01	96.94
94007	14	0.06	6.40	15.23	35.65	9.78	3.28	25.32	0.23	0.01	95.96
94007	14	0.02	6.40	15.33	36.24	9.20	3.68	25.96	0.18	0.01	97.02
94008	16	0.02	6.79	15.27	36.19	10.20	2.53	26.65	0.32	0.01	97.98
94008	16	0.13	6.51	15.22	35.97	10.13	2.87	24.23	0.24	0.01	95.31
94008	16	0.04	6.86	14.98	34.46	9.56	2.36	24.82	0.28	0.00	93.36
94009	20	0.02	12.55	15.94	36.44	9.79	2.01	17.47	0.51	0.01	94.74
94009	20	0.08	12.78	15.49	37.06	9.49	1.96	17.26	0.44	0.01	94.57
94009	20	0.04	11.93	16.4	38.43	9.85	2.14	17.79	0.39	0.01	96.98
94010	22	0.11	12.92	15.44	37.04	9.31	2.18	17.19	0.40	0.01	94.60
94010	22	0.05	12.17	15.55	38.29	9.68	2.17	17.46	0.39	0.00	95.76
94010	22	0.04	13.11	15.41	37.12	9.55	2.27	16.79	0.33	0.01	94.63
94011	24	0.05	10.81	15.44	35.49	10.39	2.40	18.30	0.41	0.00	93.29
94011	24	0.02	11.50	15.22	37.06	10.31	2.28	18.43	0.36	0.01	95.19
94011	24	0.06	11.29	15.19	37.4	9.69	2.22	18.66	0.31	0.01	94.83
94012	26	0.09	8.37	15.08	33.73	9.42	2.30	22.60	0.44	0.00	92.03
94012	26	0.01	7.92	14.99	36.22	9.81	3.02	22.17	0.35	0.01	94.50
94012	26	0.05	8.17	15.16	36.49	10.16	2.75	22.09	0.29	0.01	95.17
94013	30	0.02	5.32	14.49	33.39	9.49	2.46	23.47	0.28	0.00	88.92
94013	30	0.03	4.35	15.09	36.74	9.73	2.44	26.74	0.08	0.03	95.23
94014	32	0.04	5.01	15.32	35.86	9.47	2.67	27.85	0.22	0.00	96.44
94014	32	0.00	4.74	15.28	35.08	9.46	2.51	28.89	0.28	0.02	96.26
94014	32	0.06	4.96	15.25	35.93	9.25	2.47	27.63	0.18	0.03	95.76
94016	36	0.00	4.87	15.37	34.82	9.20	2.72	27.1	0.31	0.03	94.42
94016	36	0.03	4.64	15.65	35.28	9.26	2.95	27.42	0.12	0.03	95.38
94016	36	0.02	4.11	16.26	35.04	9.33	2.62	26.82	0.19	0.02	94.41
94020	44	0.06	3.73	15.80	34.59	9.31	2.63	27.31	0.16	0.06	93.65
94020	44	0.00	3.79	15.41	36.26	9.21	2.65	27.85	0.24	0.04	95.45
94020	44	0.06	4.09	15.84	35.46	9.63	2.80	27.03	0.10	0.00	95.01
94024	52	0.02	4.92	15.37	38.78	9.14	2.36	26.64	0.17	0.02	97.42
94024	52	0.05	4.76	15.43	36.77	9.38	2.56	27.16	0.13	0.00	96.24
94024	52	0.06	4.95	14.72	35.15	8.55	2.49	26.75	0.22	0.00	92.89
94028	66	0.06	4.85	15.00	35.15	8.88	2.73	26.6	0.22	0.01	93.50
94028	66	0.00	5.06	14.38	34.59	9.38	2.37	26.65	0.22	0.01	92.66
94028	66	0.03	4.92	15.40	36.83	9.68	2.19	27.8	0.14	0.00	96.99

App. 2.1: Muscovite analysis (concentrations in weight percent)

Sample	m from ore	Na ₂ O	MgO	Al ₂ O ₃	SiO ₂	K ₂ O	TiO ₂	FeO	F	Cl	sum
94004	8	0.21	2.48	38.69	45.87	9.05	0.07	0.43	0.22	0.01	97.03
94004	8	0.26	2.9	31.17	48.17	9.85	0.53	2.41	0.09	0.00	95.38
94004	8	0.36	2.66	30.27	50.33	9.23	0.64	2.30	0.25	0.01	96.05
94005	10	0.23	2.66	31.34	43.59	8.62	0.55	2.17	0.17	0.00	89.33
94005	10	0.33	2.79	30.74	35.97	8.65	0.71	2.19	0.19	0.01	81.58
94005	10	0.29	2.58	28.69	46.77	8.57	0.57	2.02	0.21	0.00	89.70
94005	10	0.11	2.79	19.51	53.93	8.40	0.24	1.90	0.22	0.00	87.10
94006	12	0.43	2.87	31.89	53.02	8.22	0.37	1.81	0.14	0.00	98.75
94006	12	0.28	3.63	31.08	53.42	8.54	0.39	1.86	0.11	0.00	99.31
94007	14	0.26	1.49	29.2	49.76	9.20	1.14	5.69	0.15	0.00	96.89
94007	14	0.28	1.39	29.47	48.5	8.43	1.12	6.18	0.08	0.00	95.45
94007	14	0.36	1.45	30.52	49.38	9.42	1.13	6.12	0.09	0.00	98.47
94008	16	0.38	1.40	29.98	49.59	9.30	0.67	6.54	0.14	0.00	98.00
94008	16	0.39	1.61	29.11	47.61	9.44	0.73	6.52	0.05	0.00	95.46
94008	16	0.27	1.70	28.99	47.57	8.88	0.64	6.67	0.15	0.00	94.87
94009	20	0.18	2.38	28.85	51.31	8.60	0.68	5.04	0.10	0.00	97.14
94009	20	0.28	2.11	28.85	49.46	8.72	0.69	5.16	0.13	0.00	95.40
94009	20	0.27	2.16	29.67	51.07	9.21	0.72	5.04	0.06	0.00	98.20
94010	22	0.28	2.25	28.62	47.90	8.42	1.17	5.32	0.09	0.01	94.06
94010	22	0.30	2.05	29.15	50.06	8.26	1.36	5.07	0.00	0.00	96.25
94011	24	0.26	1.89	28.88	49.43	9.41	0.96	5.68	0.08	0.00	96.59
94011	24	0.25	2.61	26.57	46.68	10.07	0.73	5.52	0.09	0.01	92.53
94011	24	0.33	2.07	28.47	47.61	10.38	0.99	5.9	0.03	0.01	95.79
94011	24	0.29	2.12	28.17	47.15	10.17	1.05	5.57	0.00	0.02	94.54
94012	26	0.27	1.67	28.53	47.86	10.48	1.15	6.31	0.19	0.00	96.46
94012	26	0.34	1.67	27.56	45.74	10.03	0.98	7.27	0.09	0.00	93.68
94012	26	0.30	1.72	28.40	47.00	10.32	1.05	9.98	0.09	0.01	98.87
94013	30	0.22	1.48	26.31	47.32	9.91	0.67	6.96	0.12	0.00	92.99
94013	30	0.24	1.52	26.57	47.48	10.31	0.71	6.97	0.04	0.00	93.84
94013	30	0.23	1.42	27.16	47.15	10.36	0.73	7.22	0.09	0.01	94.37
94014	32	0.22	1.36	27.18	46.22	9.84	0.91	7.67	0.11	0.01	93.52
94014	32	0.24	1.48	25.91	48.19	10.12	0.90	7.63	0.07	0.00	94.54
94014	32	0.24	1.37	26.21	46.43	10.42	0.93	7.75	0.10	0.01	93.46
94016	36	0.21	1.43	29.02	49.80	10.48	0.52	5.51	0.08	0.00	97.05
94016	36	0.20	1.38	28.24	48.16	10.21	0.54	5.27	0.09	0.00	94.09
94016	36	0.22	1.38	28.84	49.16	9.86	0.45	5.16	0.10	0.01	95.18
94020	44	0.18	1.41	28.84	49.89	10.48	0.39	5.75	0.06	0.00	97.00
94020	44	0.23	1.31	28.37	47.57	9.82	0.72	5.89	0.15	0.00	94.06
94020	44	0.16	1.29	29.29	47.39	9.96	0.31	5.28	0.11	0.01	93.80
94024	52	0.23	1.45	26.27	47.05	9.75	0.67	7.13	0.12	0.00	92.67
94024	52	0.22	1.42	27.3	44.78	9.42	0.67	7.22	0.18	0.00	91.21
94028	66	0.17	1.54	25.92	49.25	10.33	0.9	6.94	0.14	0.00	95.19